

Si/Ge Platform for lasers, amplifiers, and nonlinear optical devices based on the Raman Effect

Ricardo Claps
Neptec Optical Solutions
48603 Warm Springs Blvd.
Fremont, CA 94539

Dimitri Dimitropoulos, Varun Raghunathan, Sasan Fathpour, Bahram Jalali
Optoelectronics Circuits and Systems Laboratory
University of California, Los Angeles
420 Westwood Plaza
Los Angeles, CA 90095

Bernard Jusserand
Institut des Nanosciences de Paris, Universit'e Pierre et Marie Curie, UMR CNRS 7588,
Campus Boucicaut,
140 Rue de Lourmel, 75015 Paris, France

Abstract: The use of a silicon-germanium platform for the development of optically active devices will be discussed in this paper, from the perspective of Raman and Brillouin scattering phenomena. Silicon-Germanium is becoming a prevalent technology for the development of high speed CMOS transistors, with advances in several key parameters as high carrier mobility, low cost, and reduced manufacturing logistics. Traditionally, Si-Ge structures have been used in the optoelectronics arena as photodetectors, due to the enhanced absorption of Ge in the telecommunications band. Recent developments in Raman-based nonlinearities for devices based on a silicon-on-insulator platform have shed light on the possibility of using these effects in Si-Ge architectures. Lasing and amplification have been demonstrated using a SiGe alloy structure, and Brillouin/Raman activity from acoustic phonon modes in SiGe superlattices has been predicted. Moreover, new Raman-active branches and inhomogeneously broadened spectra result from optical phonon modes, offering new perspectives for optical device applications. The possibilities for an electrically-pumped Raman laser will be outlined, and the potential for design and development of silicon-based, Tera-Hertz wave emitters and/or receivers.

1. Motivation

The use of Raman nonlinear processes in silicon waveguides has emerged in the past 2 years as a promising route for the implementation of optically active devices in silicon [1, 2, 3, 4, 5, 6, 7]. There are three hard-core parameters that cannot be changed by fabrication or design, if one is bound to use bulk silicon as the main platform, these are: Raman strength, spectral bandwidth, and spectral range. The main goal of this paper is to demonstrate that the silicon-germanium platform (SGP) is a powerful tool to modify these aspects of the Raman Effect, which directly relate to their technological implementation in optical nonlinear phenomena like Stimulated Brillouin/Raman Scattering (SBRS) and Coherent anti-Stokes Raman Scattering (CARS). This offers an interesting alternative to the well-known silicon-on-insulator platform (SOI), which has been widely used recently [2-9], or GaP, which was developed several years ago by the group of Nishizawa et al, in Japan [10].

The SGP also offers a fabrication and design scheme that is currently used for high-speed CMOS and MOSFET device fabrication. Recent development of stressed-silicon layers, built on top of silicon-germanium substrates, have demonstrated the fastest MOSFET devices to-date [11], boosting the prospects for the SGP in the integrated-circuit design arena. Furthermore, by managing the ability to tune the inter-sub-band electron-hole levels in a SGSL, resonances in electron-phonon modes can be exploited to produce a fast, electrically pumped laser/amplifier.

Super-lattices based on SiGe structures have been considered in the past as a means to obtain a direct band-gap in silicon-based materials [12]. These endeavors faced the difficult issue of handling interface imperfections, especially for SL with a few monolayers in each period [13]. The defects create non-radiative electronic states which quench the optical activity of the material. It is important to note that the analysis presented in this paper will not suffer from the same problem, since Raman emission at near-Infrared wavelengths does not rely on electronic transitions. The authors have already performed the analysis of Raman/Brillouin scattering from folded acoustic phonon modes (FAPM) [1], which will be summarized in section 2.1 of the paper. Section 2.2 of the paper introduces the analysis of Raman scattering in SGSL's from folded-optical phonon modes (FOPM) in the structure. The microscopic nature of the optical modes of vibration makes them qualitatively different from acoustic modes; therefore the need to use the Bond-Polarizability-Theory to treat Raman scattering in this case.

2. Theory and Model

2.1 Brillouin/Raman Scattering from FAPM

In the case of the FAPM's, the Raman scattering resulting from these modes has its origin in the photo-elastic interaction in the same manner as bulk Brillouin scattering [1]. However, a unique property of super-lattice Brillouin Scattering is that forward scattering is allowed, because the confinement of the FAPM's provides phonon states with finite frequency at zone-center. Fig. 1 shows the geometry of the scattering configuration, where the Z-axis is chosen as that of the SGSL growth direction, the waveguide is etched along the X-axis. The phonon waves propagate along the waveguide direction, k_x , and the active wave amplitude component stretches also along the X-axis, $\Psi^{\pm N}_x$. These Brillouin active modes come in pairs, or "doublets", denoted by the sign \pm , depending on which side of the frequency gap they are located. The integer, N, indicates the order of zone-folding for the specific wave.

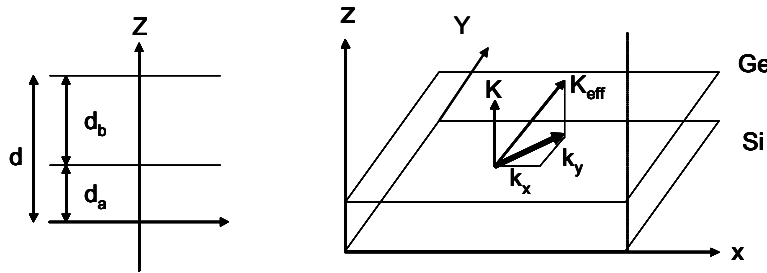


FIG. 1. Geometry selected for the analysis of the SGSL. A germanium layer of thickness, d_b , is grown on top of a silicon layer of thickness, d_a . Plane waves propagating in the xy plane acquire a momentum component, K , along the z -direction, as expressed in Bloch's theorem.

The optical spectrum of the Ψ^{\pm}_x -FAPMs, is depicted in Fig.2, as it changes with respect to the relative thickness between the Si and Ge layers. The scattering configuration is denoted by X(ZZ)X. A lorentzian linewidth of 6 GHz has been assumed for all the modes. Notice the

spectral resolution required to distinguish between the two components of a doublet line (< 100 GHz).

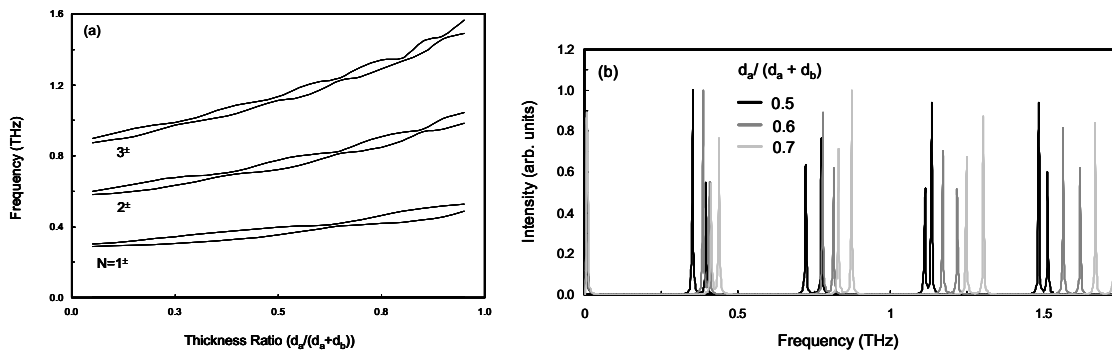


FIG. 2 (a) Variation of the Brillouin-active mode frequencies with respect to the relative thickness of the silicon-germanium layers. (b) Frequency spectrum of Brillouin/Raman peaks from the SGSL at zone-center, for different silicon layer thicknesses. The spectral shift for the specific case of the doublets, $N=2, 3, 4$, given three values of $d_a/(d_a+d_b)=0.5, 0.6, 0.7$. The frequency shift is not homogeneous, but the spectral features are preserved.

Figures 2 and 3 show that optical scattering from Raman active acoustic phonon modes in SGSL offers an opportunity to modify the spectrum of Raman based silicon waveguide devices. It is found that a “bandgap pinching” effect [1] leads to specific layer thicknesses for Si and Ge that optimize the efficiency of the optical process. A clear resonance condition is identified for $d_a/d=0.65$. In sum, the Brillouin/Raman spectrum constitutes a comb-frequency profile whose frequency spacing (or “free spectral range”) can be adjusted by design. The adjustment is achieved by tailoring the relative thicknesses of the Si and Ge layers in the SGSL.

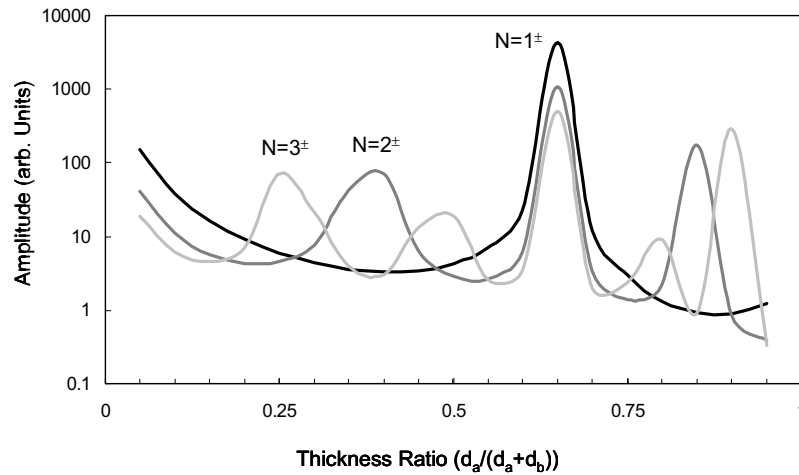


FIG. 3 Relative intensity of Brillouin scattering, from a SGSL with varying relative thickness of Si and Ge. The curves are obtained using Eq. (8), and Eq. (9) for the bandgap calculation. Notice the resonance, for all N, at $d_a = 0.65$.

2.2- Raman scattering from FOPM

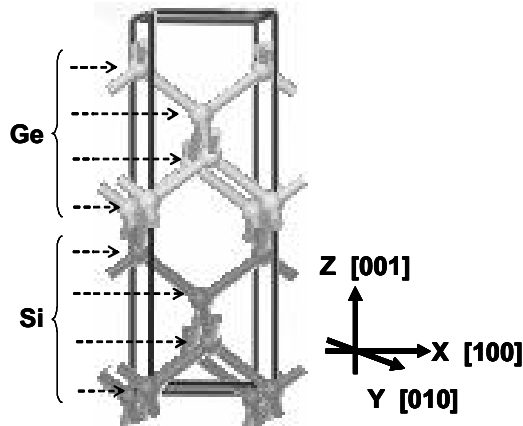


FIG. 4 Unit Cell of the Si_4Ge_4 super-lattice used in the simulations presented in the paper. The cell has been optimized using CASTEP, so the atom positions correspond to the equilibrium values. The bond length is 2.14 Å, the lateral cell size is 3.82 Å (x,y) and height is 10.95 Å (z).

The Raman spectra of SGSL's along the plane normal to the growth direction (in-plane propagating phonons) have been studied in the past [14, 15, 16]. Since this direction is not a high-symmetry axis of the SL, several optical phonon modes become Raman-active in this scattering configuration. This attracted many authors with the idea of using the Raman spectra thus obtained in order to extract information about the geometry and strain in the SL, as well as providing critical information about interface roughness [17].

In this work, the emphasis will be on the use of the newly generated Raman-active phonon modes to improve the performance of Raman-based nonlinear optical devices, like signal amplifiers, lasers, and wavelength converters. The following

discussion will be limited to a Si_4Ge_4 super-lattice composed of 4 layers of Si and 4 layers of Ge, without consideration of boundary conditions. The unit cell of the structure is shown in Fig. 4; it is composed of 8 atoms. Zone-folding in Si/Ge SL's grown along the [001] direction is discussed and described in detail in [18] and references therein. The dispersion relation obtained for the Si_4Ge_4 structure using the software package, CASTEP [19], is depicted in Fig. 5, for two directions of propagation: in plane propagation [010], and along the direction of growth of the SL, [001].

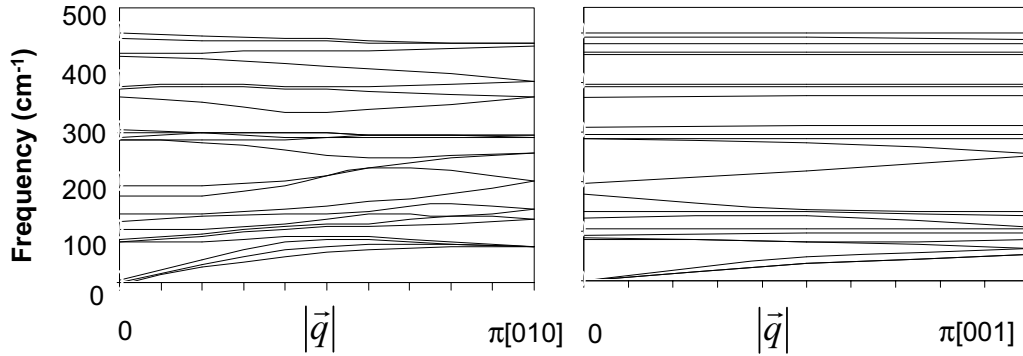


FIG. 5 Phonon dispersion curves for the Si_4Ge_4 SL, shown in Fig. 4. The modes that will be of interest for this work are shown to the left, and propagate along the plane of the layered structure ([010] direction). Furthermore, the Raman-active modes are the ones at the Gamma point ($q=0 \text{ cm}^{-1}$).

The zone-folding effect is clearly apparent in both cases, although there is more dispersion for phonons propagating along the [010] direction. For calculating the phonon displacement vectors in the Si_4Ge_4 superlattice, a linear chain approximation has been used. In this scheme, each layer along the [001] direction is treated as a single body, exerting restoring forces on the nearest neighbor layer. The phonon mode, propagating along [001], can be pictured as an 8-component vector, \vec{u} , each component corresponding to the displacement of a single atomic layer. The equation of motion (harmonic approximation) is written as:

$$\vec{D} \cdot \vec{u} = -\omega^2 \vec{u} \quad . \quad (1)$$

Where, D , is the dynamical matrix of the system. The dynamical matrices for propagation along [001] are calculated as in Ref. [18] and they are explicitly shown below. One of the relevant parameters is the relative mass of the silicon and germanium layers, m_a and m_b , respectively. Three force field coefficients, f , f_1 and f_2 are chosen such that the phonon frequencies derived from solving the dynamic equation, for phonon propagation vector, $\vec{q}=0$, match the experimentally observed values. The validity of the approach followed is established by verifying that the 24 phonon modes obtained belong to the B_{1u} representation of the symmetry group of the Si_4Ge_4 super lattice D_{2h}^5 [20].

Longitudinal Modes:

$$\mathbf{D}^L = \begin{pmatrix} \frac{2f}{m_a} & \frac{-f}{m_a} & 0 & 0 & 0 & 0 & 0 & \frac{-e^{-idk}f}{m_a} \\ \frac{-f}{m_a} & \frac{2f}{m_a} & \frac{-f}{\sqrt{m_b m_a}} & 0 & 0 & 0 & 0 & 0 \\ 0 & \frac{-f}{\sqrt{m_b m_a}} & \frac{2f}{m_b} & \frac{-f}{m_b} & 0 & 0 & 0 & 0 \\ 0 & 0 & \frac{-f}{m_b} & \frac{2f}{m_b} & \frac{-f}{m_b} & 0 & 0 & 0 \\ 0 & 0 & 0 & \frac{-f}{m_b} & \frac{2f}{m_b} & \frac{-f}{m_b} & 0 & 0 \\ 0 & 0 & 0 & 0 & \frac{-f}{m_b} & \frac{2f}{m_b} & \frac{-f}{\sqrt{m_b m_a}} & 0 \\ 0 & 0 & 0 & 0 & 0 & \frac{-f}{\sqrt{m_b m_a}} & \frac{2f}{m_a} & \frac{-f}{m_a} \\ \frac{-e^{idk}f}{m_a} & 0 & 0 & 0 & 0 & 0 & \frac{-f}{m_a} & \frac{2f}{m_a} \end{pmatrix}.$$

Transversal modes (1):

$$\mathbf{D}^{T1} = \begin{pmatrix} \frac{(f_1+f_2)}{m_a} & \frac{-f_1}{m_a} & 0 & 0 & 0 & 0 & 0 & \frac{-e^{-idk}f_2}{m_a} \\ \frac{-f_1}{m_a} & \frac{(f_1+f_2)}{m_a} & \frac{-f_2}{\sqrt{m_b m_a}} & 0 & 0 & 0 & 0 & 0 \\ 0 & \frac{-f_2}{\sqrt{m_b m_a}} & \frac{(f_1+f_2)}{m_b} & \frac{-f_1}{m_b} & 0 & 0 & 0 & 0 \\ 0 & 0 & \frac{-f_1}{m_b} & \frac{(f_1+f_2)}{m_b} & \frac{-f_2}{m_b} & 0 & 0 & 0 \\ 0 & 0 & 0 & \frac{-f_2}{m_b} & \frac{(f_1+f_2)}{m_b} & \frac{-f_1}{m_b} & 0 & 0 \\ 0 & 0 & 0 & 0 & \frac{-f_1}{m_b} & \frac{(f_1+f_2)}{m_b} & \frac{-f_2}{\sqrt{m_b m_a}} & 0 \\ 0 & 0 & 0 & 0 & 0 & \frac{-f_2}{\sqrt{m_b m_a}} & \frac{(f_1+f_2)}{m_a} & \frac{-f_1}{m_a} \\ \frac{-e^{idk}f_2}{m_a} & 0 & 0 & 0 & 0 & 0 & \frac{-f_1}{m_a} & \frac{(f_1+f_2)}{m_a} \end{pmatrix}$$

$$\mathbf{D}^{T1} = \begin{pmatrix} \frac{(f_1+f_2)}{m_a} & \frac{-f_2}{m_a} & 0 & 0 & 0 & 0 & 0 & \frac{-e^{-idk}f_2}{m_a} \\ \frac{-f_2}{m_a} & \frac{(f_1+f_2)}{m_a} & \frac{-f_1}{\sqrt{m_b m_a}} & 0 & 0 & 0 & 0 & 0 \\ 0 & \frac{-f_1}{\sqrt{m_b m_a}} & \frac{(f_1+f_2)}{m_b} & \frac{-f_2}{m_b} & 0 & 0 & 0 & 0 \\ 0 & 0 & \frac{-f_2}{m_b} & \frac{(f_1+f_2)}{m_b} & \frac{-f_1}{m_b} & 0 & 0 & 0 \\ 0 & 0 & 0 & \frac{-f_1}{m_b} & \frac{(f_1+f_2)}{m_b} & \frac{-f_2}{m_b} & 0 & 0 \\ 0 & 0 & 0 & 0 & \frac{-f_2}{m_b} & \frac{(f_1+f_2)}{m_b} & \frac{-f_1}{\sqrt{m_b m_a}} & 0 \\ 0 & 0 & 0 & 0 & 0 & \frac{-f_1}{\sqrt{m_b m_a}} & \frac{(f_1+f_2)}{m_a} & \frac{-f_2}{m_a} \\ \frac{-e^{idk}f_2}{m_a} & 0 & 0 & 0 & 0 & 0 & \frac{-f_2}{m_a} & \frac{(f_1+f_2)}{m_a} \end{pmatrix}.$$

2.1- Bond Polarizability Theory

Typical calculations of the Raman scattering coefficients in complex systems like superlattices, alloys, and so on, are based in the so-called Bond Polarizability Theory (BPT) [21-23]. This model assumes that the ions in a covalent lattice are bonded by elongated, p-type electronic orbital states, which in essence act as springs, holding the ions together. These “springs” have a polarizability, α , associated with them, which in general has two components: an isotropic component, α_{\parallel} ; and α_{\perp} , which is the anisotropic, “de-polarizing” component, whereby a field applied in a given direction induces a dipole moment in an orthogonal direction.

Following [21], let \mathbf{r}_i be the equilibrium position and \mathbf{u}_i^j the displacement of the i -th ion, for the j -th phonon mode in a lattice, and let $\mathbf{R}_i^j = \mathbf{r}_i + \mathbf{u}_i^j$. The bond properties are defined by vectors of the form $\mathbf{R}_{ik}^j = \mathbf{R}_i^j - \mathbf{R}_k^j$, and so on, where the ik -bond is that joining ions i and k . Vectors \mathbf{r}_{ik} and \mathbf{u}_{ik}^j are defined likewise. The total polarizability, $\mathbf{P}_{\mu\nu}(\mathbf{R}_{ik}^j)$, of the ik bond associated to the j -th phonon mode, is written as,

$$P_{\mu\nu}(R_{ik}^j) = \alpha_{\parallel}(R_{ik}^j)\bar{I}_{\mu\nu} + \alpha_{\perp}(R_{ik}^j)(\hat{R}_{ik}^j\hat{R}_{ik}^j - 1/3 \cdot \bar{I})_{\mu\nu}$$

$$\vec{P}_{\mu} = P_{\sigma\nu}\vec{E}_{\nu}; \quad \vec{E}_{\nu} \rightarrow \text{External Electric Field}; \quad \vec{P}_{\nu} \rightarrow \text{Induced Dipole Moment.} \quad (2)$$

$$\bar{I}_{\mu\nu} \rightarrow \text{Identity Tensor}$$

Assuming $u_{ik}^j \ll r_{ik}$ for any and all phonon modes, j , and expressing $\mathbf{P}_{\mu\nu}(\mathbf{R}_{ik}^j)$ in powers of u_{ik}^j using a first-order Taylor expansion, we arrive at

$$P_{\mu\nu}(R_{ik}^j) = (\vec{u}_{ik}^j \cdot \hat{r}_{ik}) \cdot \{ \partial_j \alpha_{\parallel} \bar{I}_{\mu\nu} + \partial_j \alpha_{\perp} (\hat{r}_{ik} \hat{r}_{ik} - 1/3 \cdot \bar{I})_{\mu\nu} \}$$

$$+ r_{ik}^{-1} \alpha_{\perp}(r_{ik}) \cdot \{ \vec{u}_{ik}^j \hat{r}_{ik} + \hat{r}_{ik} \vec{u}_{ik}^j - 2(\vec{u}_{ik}^j \cdot \hat{r}_{ik}) \hat{r}_{ik} \hat{r}_{ik} \}_{\mu\nu}, \quad (3)$$

where no summation should be assumed for repeated indices, and the derivative operator, ∂_j , is carried out with respect to the component R_{ik}^j . The next step is to take the direct sum of expression (3) for each of the bonds in the unit cell of the crystal structure, and arrive finally at a polarizability tensor, $\mathbf{P}^{(j)}$, of the form

$$P^{(j)} = \sum_{ik} P(R_{ik}^j) = \begin{pmatrix} P_{xx}^j & P_{xy}^j & P_{xz}^j \\ P_{xy}^j & P_{yy}^j & P_{yz}^j \\ P_{xz}^j & P_{yz}^j & P_{zz}^j \end{pmatrix}. \quad (4)$$

Note that Eq.(4) contains the information of the j -th phonon mode of vibration of the structure, and more importantly, it is written in the most general fashion regarding the symmetry expected for a SGSL grown along the z -axis [24]. Since the analysis has the symmetry of the SL crystal built in, the modes that will become Raman active are automatically accounted for. The key result is that the number of Raman-active optical-

phonon modes at zone center is increased, as will be shown below. This behavior offers the ability to engineer the spectrum of Raman gain and nonlinear susceptibility, and hence to remove the spectrum limitation of Raman scattering in bulk silicon. For a given phonon mode, the sum over the bonds along the unit cell in Eq. (4) can be taken along each of the layers of the SL structure. The assumption is made that, for each atom in the unit cell, the polarizability and its derivatives are given by the bulk value of the material involved in that layer. This is a major hypothesis that can only be verified by an ab-initio calculation, or matching the calculated spectra to experimental data. The total scattering intensity involves the temperature-dependent Bose-Einstein population factor, $n(\omega)$, and an assumption of a Lorentzian line-shape for each of the phonons in the structure [24]. The spectrum is therefore given by

$$I(\omega) \propto \sum_j \frac{\Gamma / \pi}{(\omega - \omega_j)^2 + \Gamma^2} (P_{zz}^{(j)} + P_{yz}^{(j)}) \frac{n(\omega_j) + 1}{\omega_j}, \quad (5)$$

where P_{yz}^j is the scattering intensity with pump and Stokes fields oriented along z and y, respectively. The summation over j takes into account the normal phonon modes. The task left is to find the appropriate values of the coefficients, $\{\partial\alpha_{\parallel}, \partial\alpha_{\perp}, \alpha_{\perp}, \alpha_{\parallel}\}$, for each of the ionic layers: Si and Ge. The values given in Table 1 below have been measured at a pump wavelength $\lambda_p = 488$ nm [23-25]. Clearly, these values should be corrected for the wavelength of interest, given the specific application and device design that is sought. For the purposes of the present work, since only the relative peak intensities are of interest, it will be assumed that the ratio of the coefficients for Si and Ge are kept constant for different wavelengths. Thus the values from Table 1 will be used with no correction for λ_p .

Table I
Bond-Polarizability constants of Si and Ge^{a,b}

	Si	Ge	[]
α_{\odot}	6	9.89	A^3
$\alpha_{\gamma\gamma}$	7.75	15.5	A^3
α_{xx}	3.32	9.93	
α_{xy}	1.59	4.07	
$\partial \alpha_{\odot}$	3.01	8.80	$\frac{\sqrt{3}}{2}\alpha_{xx} + \frac{2}{3\sqrt{3}}\alpha_{\perp}$
$\partial \alpha_{\gamma\gamma}$	-3.80	-10.12	$\frac{-3\sqrt{3}}{2}\alpha_{xy} + \frac{2}{\sqrt{3}}\alpha_{\parallel}$

^a S. Go, H. Bilz, M. Cardona; "Bond Charge, Bond Polarizability, and Phonon Spectra in Semiconductors", Phys. Rev. Lett. **34**(10) 580 (1975).

^b M.W.C. Dharma-Wardana, G.C. Aers, D.J. Lockwood, J.M. Baribeau; "Interpretation of Raman spectra of Si/Ge ultrathin superlattices", Phys. Rev. B **41**(8) 5319 (1990).

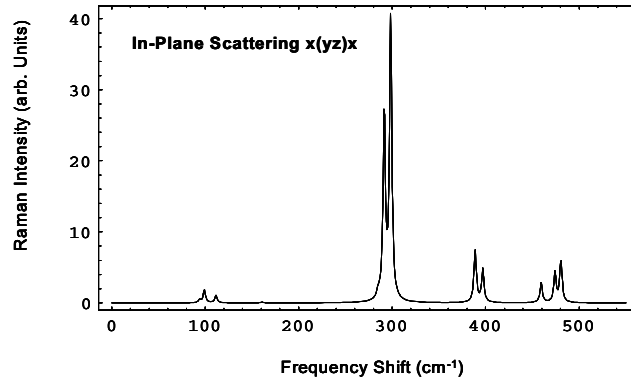


FIG. 6 Raman spectrum from the Si₄Ge₄ SL as derived from Eq. (4) and Eq. (5) and using the coefficients listed in Table 1. The phonon modes used correspond to the Gamma point modes shown in Fig. 2 above.

3.- Results and Discussion

The resulting Raman spectrum is shown in Fig. 6, above. Two points from that figure need to be stressed. On one hand, a large Raman peak is observed at $\sim 300 \text{ cm}^{-1}$, corresponding to the optical phonon branch of germanium. This peak is considerably stronger than the Si peak, and is located much closer to the pump wavelength, which makes it a very convenient candidate for an amplifier or a wavelength converter. Another important point is that, as a result of the appearance of new optical modes near the Si branch, an inhomogeneously-broadened line results at $\sim 490 \text{ cm}^{-1}$.

Stress becomes an issue for all instances in which a SGP is involved, due to the 4% lattice constant mismatch between Si and Ge. In the case of Raman scattering from optical phonon modes, the effect of stress has been well documented and studied in the past three decades [20, 26, 27]. These references conclude that, in general, the effect of uniaxial stress on the spectrum will be a linear shift of the Raman frequencies by about 1 to 2 cm^{-1} per GPa. This effect is of no considerable impact for the purposes discussed in this paper. However, there is also a spectral splitting of the Raman-active triplets into a singlet phonon, with polarization aligned with the direction of the stress, and a doublet phonon state, with polarization aligned in the plane perpendicular to this direction. This splitting is comparable, but smaller, than the stress-induced shift. The net result is a reduction of the Raman peak intensity and an increase in its bandwidth. The practical implications of this should be explored further, although they lay out of the scope of the present work.

3. Electrically Pumped Brillouin-Raman laser

Using the high electron-hole mobility that can be achieved with a silicon-germanium-on-insulator platform, extremely fast electronic currents can be generated in the structure. These currents will not interact with thermal acoustic phonons in the lattice, but will have a larger scattering cross-section with higher order acoustic modes ($N \gg 1$), if the electronic levels in the conduction band of the SiGe SL are carefully designed to match the frequency of one of the FAPM. This has been suggested and successfully demonstrated in the case of Quantum Cascade Laser emitters in the THz domain [28].

Electron-Phonon scattering processes will be used to generate Brillouin-active acoustic phonon waves. By enhancing the amplitude of these waves in this manner, the effective Brillouin efficiency is increased and lasing occurs, once the amplification threshold is reached.

4. Conclusion and Outlook

We have demonstrated that the Brillouin/Raman scattering process is possible for SGSL structures using in-plane scattering configurations. More importantly, it has been demonstrated that the Brillouin spectrum constitutes a comb-frequency profile that can be adjusted in frequency spacing (or “free spectral range”), and separation range from the pump frequency. The adjustment is simply performed by tailoring the relative thicknesses of the Si and Ge layers in the SGSL. This property of Brillouin/Raman scattering from a SGSL-based waveguide can be used to generate and detect Tera-Hertz electromagnetic radiation. Using the Bond-Polarizability Theory, for the case of in-plane Raman scattering from a Si_4Ge_4 SL, the appearance of several Raman-active optical phonon modes has been demonstrated. This can be used to enhance the spectral performance of a Raman-based amplifier, laser, and/or wavelength converter. A high intensity Raman mode at 300 cm^{-1} is predicted to exist, mainly coming from the optical phonon mode of bulk germanium. The bulk-silicon mode is shifted to lower frequencies by $\sim 30 \text{ cm}^{-1}$, and is inhomogeneously broadened. Finally, the prospects for realizing an electrically-pumped, Brillouin/Raman laser, have been suggested based on the electron-phonon scattering cross-sections of SiGe super-lattices.

References

- [1] R. Claps, D. Dimitropoulos, B. Jalali and B. Jusserand; "Raman scattering from acoustic modes in Si/Ge superlattice waveguides", *Superlattices and Microstructures* **39** 501-506 (2006).
- [2] R. Claps, D. Dimitropoulos, V. Raghunathan, Y. Han, and B. Jalali, "Observation of stimulated Raman amplification in silicon waveguides," *Opt. Express* **11**, 1731-1739 (2003),
<http://www.opticsexpress.org/abstract.cfm?URI=OPEX-11-15-1731>
- [3] R. Claps, V. Raghunathan, D. Dimitropoulos, and B. Jalali, "Anti-Stokes Raman conversion in silicon waveguides," *Opt. Express* **11**, 2862-2872 (2003),
<http://www.opticsexpress.org/abstract.cfm?URI=OPEX-11-22-2862>
- [4] V. Raghunathan, R. Claps, D. Dimitropoulos, B. Jalali; "Wavelength conversion in silicon using Raman induced four wave mixing", *Appl. Phys. Lett.* **85** (34) (2004)
- [5] O. Boyraz, T. Indukuri, and B. Jalali, "Self-phase-modulation induced spectral broadening in silicon waveguides," *Opt. Express* **12**, 829-834 (2004),
<http://www.opticsexpress.org/abstract.cfm?URI=OPEX-12-5-829>
- [6] Q. Xu, V. R. Almeida, and M. Lipson, "Time-resolved study of Raman gain in highly confined silicon-on-insulator waveguides," *Opt. Express* **12**, 4437-4442 (2004),
<http://www.opticsexpress.org/abstract.cfm?URI=OPEX-12-19-4437>
- [7] R. L. Espinola, J. I. Dadap, R. M. Osgood, Jr., S. J. McNab, and Y. A. Vlasov, "Raman amplification in ultrasmall silicon-on-insulator wire waveguides," *Opt. Express* **12**, 3713-3718 (2004),
<http://www.opticsexpress.org/abstract.cfm?URI=OPEX-12-16-3713>
- [8] Liang TK, Tsang HK; "Efficient Raman amplification in silicon-on-insulator waveguides", *Appl. Phys. Lett.* **85** (16), 3343-3345 (2004).
- [9] Rong HS, Liu AS, Nicolaescu R, Paniccia M, Cohen O, Hak D; "Raman gain and nonlinear optical absorption measurements in a low-loss silicon waveguide", *Appl. Phys. Lett.* **85** (12), 2196-2198 (2004).
- [10] Ken Suto and Jun-Ichi Nishizawa; **Semiconductor Raman Lasers**, Artech House, Boston-London, ISBN 0-89006-667-1 (1994).
- [11] D. Harame, et al; "The revolution in SiGe: Impact on device electronics", *Applied Surface Science*, **224**, 9-17 (2004).
- [12] T.P. Pearsall, J. Bevk, L.C. Feldman, J.M. Bonar, J.P. Mannaerts, A. Ourmazd; "Structurally Induced Optical Transitions in Ge-Si superlattices" *Phys. Rev. Lett.* **58**, 729 (1987).
- [13] U. Menczigar, G. Abstreiter, J. Olajos, H. Grimmeis, H. Kibbel, H. Presting; "Enhanced band-gap luminescence in strain-symmetrized $(\text{Si})_m/(\text{Ge})_n$ superlattices" *Phys. Rev. B* **47**(4)4099(1993).
- [14] R. Schorer, G. Abstreiter, S. de Gironcoli, E. Molinari, H. Kibbel, H. Presting; "In-plane Raman scattering of (001)-Si/Ge superlattices: Theory and experiment" *Phys. Rev. B* **49**(8) 5406(1994).
- [15] M.W. C. Dharma-Wardana, D.J. Lockwood, G. C. Aers, J.M. Baribeau; *J. Phys.: Condens. Matter* **1**, 2445 (1989).

- [16] S. De Gironcoli, E. Molinari; "Optical phonon probes of the lateral scale of interface roughness: a theoretical investigation", *Sol. State Electron.* **37**(4-6) 621-624 (1994).
- [17] E. Molinari, A. Fasolino; "Calculated phonon spectra of Si/Ge (001) superlattices: Features for interface characterization" *Appl. Phys. Lett.* **54**(13) 1220 (1989).
- [18] P Yu, M. Cardona; **Fundamentals of Semiconductors**, Springer-Verlag (2001).
- [19] M. D. Segall, P. J. D. Lindan, M. J. Probert, C. J. Pickard, P. J. Hasnip, S. J. Clark, M. C. Payne; "First-principles simulation: ideas, illustrations and the CASTEP code", *J. Phys.: Cond. Matt.* **14**(11) pp.2717-2743 (2002).
- [20] J. Zi, K. Zhang, X. Xie; "Phonon and Raman spectra: effect of interface diffusion of strained Si/Ge superlattices", *J. Phys. Condens. Matter* **3** 6239 (1991).
- [21] M. Cardona, G. Guntherodt; *Light Scattering in Solids V: Superlattices and Other Microstructures*, in **Topics in Applied Physics**, V. 66, Springer Verlag, Berlin (1989).
- [22] B. Zhu and K.A. Chao; "Phonon modes and Raman scattering in GaAs/Ga_{1-x}Al_xAs" *Phys. Rev. B* **36** (9) 4906 (1987).
- [23] S. Go, H. Bilz, and M. Cardona; "Bond Charge, Bond Polarizability, and Phonon Spectra in Semiconductors", *Phys. Rev. Lett.* **34**(10) 580 (1975).
- [24] E.L.Ivchenko, G.Pikus; **Superlattices and Other Heterostructures** (Symmetry and Optical Phenomena), Springer-Verlag, Berlin-Heidelberg, 1995. ISBN 3-540-58197-9.
- [25] M.W.C. Dharma-wardana, G.C. Aers, D. J. Lockwood and J.M. Baribeau, "Interpretation of Raman Spectra of Ge/Si ultrathin superlattices", *Phys. Rev B* **41** 5319 (1990).
- [26] E. Anastassakis, A. Pinczuk, E. Burstein; "Effect of uniaxial stress on the Raman spectrum of silicon", *Sol. State Comm.* **8** 133-138 (1970).
- [27] S. Nakashima, T. Mitani, M. Ninomiya, K. Matsumoto; "Raman investigation of strain in Si/SiGe Hterostructures: Precise determination of the strain-shift coefficient of Si bands"; *J. Appl. Phys.* **99** 053512 (2006).
- [28]] Menon VM, Goodhue WD, Karakashian AS, Ram-Mohan LR; "Phonon mediated lifetimes in intersubband terahertz lasers", *J. APPL. PHYS.* **88** (9): 5262-5267 (2000).